Accepted Manuscript

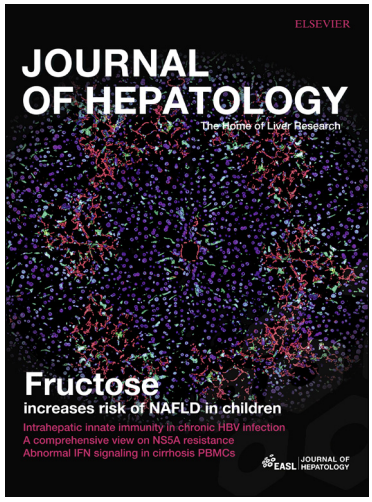

Spatial and temporal clonal evolution of intrahepatic cholangiocarcinoma

Liang-Qing Dong, Yang Shi, Li-Jie Ma, Liu-Xiao Yang, Xiao-Ying Wang, Shu Zhang, Zhi-Chao Wang, Meng Duan, Zhao Zhang, Long-Zi Liu, Bo-Hao Zheng, Zhen-Bin Ding, Ai-Wu Ke, Da-Ming Gao, Ke Yuan, Jian Zhou, Jia Fan, Ruibin Xi, Qiang Gao

PII: S0168-8278(18)30167-3
DOI: https://doi.org/10.1016/j.jhep.2018.02.029
Reference: JHEPAT 6898

To appear in: *Journal of Hepatology*

Received Date: 9 December 2017
Revised Date: 5 February 2018
Accepted Date: 12 February 2018

Please cite this article as: Dong, L-Q., Shi, Y., Ma, L-J., Yang, L-X., Wang, X-Y., Zhang, S., Wang, Z-C., Duan, M., Zhang, Z., Liu, L-Z., Zheng, B-H., Ding, Z-B., Ke, A-W., Gao, D-M., Yuan, K., Zhou, J., Fan, J., Xi, R., Gao, Q., Spatial and temporal clonal evolution of intrahepatic cholangiocarcinoma, *Journal of Hepatology* (2018), doi: https://doi.org/10.1016/j.jhep.2018.02.029

Spatial and temporal clonal evolution of intrahepatic cholangiocarcinoma

Liang-Qing Dong[1†] , Yang Shi[2†], Li-Jie Ma[1†], Liu-Xiao Yang[1], Xiao-Ying Wang[1], Shu Zhang[1], Zhi-Chao Wang[1], Meng Duan[1], Zhao Zhang[1], Long-Zi Liu[1], Bo-Hao Zheng[1], Zhen-Bin Ding[1], Ai-Wu Ke[1], Da-Ming Gao[3], Ke Yuan[4], Jian Zhou[1,5], Jia Fan[1,5*], Ruibin Xi[6*], Qiang Gao[1,7*]

Author's affiliations

(1) Department of Liver Surgery and Transplantation, Liver Cancer Institute, Zhongshan Hospital, and Key Laboratory of Carcinogenesis and Cancer Invasion (Ministry of Education), Fudan University, Shanghai 200032, China

(2) Peking-Tsinghua Center for Life Sciences, Academy for Advanced Interdisciplinary Studies, Peking University, Beijing, 100871, China

(3) CAS Key Laboratory of Systems Biology, Innovation Center for Cell Signaling Network, CAS Center for Excellence in Molecular Cell Science, Institute of Biochemistry and Cell Biology, Shanghai Institutes for Biological Sciences, Chinese Academy of Sciences,Shanghai, China;

(4) School of Computing Science and Institute of Cancer Science, University of Glasgow

(5) Cancer Center, Institute of Biomedical Sciences, Fudan University, Shanghai 200032, China;

(6) School of Mathematical Sciences and Center for Statistical Science, Peking University, Beijing, China

[(7)] State Key Laboratory of Genetic Engineering, Fudan University, Shanghai 200433, China

[†]These authors contributed equally to this work.

[*]**Corresponding authors**

Qiang Gao, MD, PhD, Department of Liver Surgery and Transplantation, Liver Cancer Institute, Zhongshan Hospital, Fudan University, 180 Fenglin Road, Shanghai 200032, China. E-mail: gaoqiang@fudan.edu.cn; Tel/fax: +86 21 64037181

Ruibin Xi, PhD, School of Mathematical Sciences and Center for Statistical Science, Peking University, 5 Yiheyuan Road, Beijing, 100871 China. E-mail: ruibinxi@math.pku.edu.cn

Jia Fan, MD, PhD, Department of Liver Surgery and Transplantation, Liver Cancer Institute, Zhongshan Hospital, Fudan University, 180 Fenglin Road, Shanghai 200032, China. E-mail: fan.jia@zs-hospital.sh.cn

Keywords: Intrahepatic cholangiocarcinoma, Whole exome sequencing, Patient-derived primary cancer cells, Clonal evolution, Intratumor heterogeneity, Branch evolution

List of abbreviations: ICC: intrahepatic cholangiocarcinoma; ITH: intratumoral heterogeneity; PDPCs: patient-derived primary cancer cells; WES: whole-exome sequencing; SNV: single nucleotide variant; CNA: copy number alteration; CCF: cancer cell fraction; CIN: chromosomal instability; GD: genome doubling; wGII: weighted Genome Instability Index; MSI: microsatellite instability; LOH: loss of

heterozygosity; FDA: food and drug administration.

Electronic word count : 5862 words

Number of figures and tables: 6 figures and no tables, 8 supplementary figures and 6 supplementary tables.

Conflict of interest statement: The authors disclose no conflicts of interest.

Financial support statement:

Supported by the National Natural Science Foundation of China (Nos. 81572292 and 81522036), Basic Research Project from Technology Commission of Shanghai Municipality (No. 17JC1402200), and National Program for Special Support of Eminent Professionals and Science.

Authors contributions:

L.Q.D, Y.S, L.J.M, J.F, R.B.X and Q.G provided clinical concept and study design; L.X.Y, W.X.Y, Z.B.D, A.W.K, J.Z, J.F and Q.G performed liver surgeries and collected fresh samples; L.J.M, Z.C.W, Z.Z, M.D, L.Z.L, B.H.Z and Q.G conducted the primary cell culture; Y.S, S.Z, K.Y, R.B.X and Q.G performed sequencing and acquisition of data; L.Q.D, L.J.M, Z.C.W, Z.Z, M.D, L.Z.L, B.H.Z, D.M.G and Q.G conducted biochemical and cellular experiments; L.Q.D, Y.S, L.J.M, K.Y, R.B.X and Q.G analyzed data; L.Q.D, Y.S, R.B.X and Q.G wrote the paper; J.F, R.B.X and Q.G were in charge of study supervision.

ABSTRACT

Background & Aims: Intrahepatic cholangiocarcinoma (ICC) is the second-most lethal primary liver cancer. Little is known about intratumoral heterogeneity (ITH) and its impact on ICC progression. We aim to investigate its ITH in hope of helping develop new therapeutic strategies.

Methods: We obtained 69 spatially distinct regions from 6 operable ICCs. Patient-derived primary cancer cells (PDPCs) were established for each region, followed by whole-exome sequencing(WES) and multi-level validation.

Results: We observed widespread ITH for both somatic mutations and clonal architecture, shaped by multiple mechanisms, like clonal "illusion", parallel evolution and chromosome instability. A median of 60.3% mutations were heterogeneous mutations, among which 85% of the driver mutations located on the branches of tumor phylogenetic trees. Many truncal and clonal driver mutations occurred in tumor-suppressor genes, such as TP53, SMARCB1 and PBRM1 that involved in DNA repair and chromatin-remodeling. Genome doubling occurred in most cases (5/6) after the accumulation of truncal mutations and was shared by all intratumoral subregions. In all cases, ongoing chromosomal instability is evident throughout the evolutionary trajectory of ICC. The recurrence of ICC1239 provided evidence to support the polyclonal metastatic seeding in ICC. The change of mutation landscape and internal diversity among subclones during metastasis, such as the loss of chemoresistance mediator, may be used for new treatment strategy. Targeted therapy against truncal alterations, such as IDH1, JAK1, and KRAS mutations and EGFR amplification, could be developed in 5/6 patients.

Conclusions: Integrated investigations of spatial ITH and clonal evolution may provide an important molecular foundation for enhanced understanding of tumorigenesis and progression in ICC.

Lay summary

We applied multiregional whole exome sequencing to investigate the evolution trajectory of ICC. The results revealed that many fuels, such as parallel evolution and chromosome instability, may participate and promote the branch diversity of ICC. Interestingly, in one patient with primary and recurrent metastatic tumors, we found some clues of polyclonal metastatic seeding, indicating that symbiotic communities of multiple clones existed and

were maintained during metastasis. More realistically, some truncal alterations, such as IDH1, JAK1, and KRAS mutations and EGFR amplification, can be promising treatment targets for ICC patients.

Introduction

Intrahepatic cholangiocarcinoma is the second most frequent type of primary liver cancer with an increasing global incidence during the past decades. Although hepatectomy is the curative method for early ICC, 5-year survival rate after resection wavers around 30-35% [1]. For those in the late stage that only receive cisplatin-based chemotherapy, the median overall survival is as low as 11.7 months[2]. The lack of commonly-accepted effective of medical care highlights the importance of understanding the ICC pathogenesis to develop new treatment strategies[3].

Recently, genomic sequencing studies have taken insights into the genetic landscape of ICC[4-6]. The driver alterations identified in ICC may represent potential candidates for personalized targeted therapy. However, genomic alterations identified in most of these studies were obtained by single sampling in individual cases, and little is known about the spatial ITH or temporal clonal evolutionary processes in ICC. In fact, anti-tumor drug development may require not only an understanding of genetic alterations but also an apprehension of the clonal status of driver alterations and evolutionary processes. During tumor progression, accumulating somatic mutations bestow a selective advantage on subclonal expansion, through which the fittest subclone will dominate. In turn, the presence of subclonal mutations may affect the efficacy of the targeted therapy. For example, in BRAFV600-mutant melanoma, the subclonal heterogeneity of PI3K-PTEN-AKT signaling are involved in the resistance to BRAF inhibitors[7]. Therefore, therapeutics targeting clonal somatic events or combination of multiple target sites seems to be more effective.

Studies adopting multiregional WES have unveiled the complex ITH and evolution pattern in several types of cancer, including prostate cancer, hepatocellular carcinoma and non-small cell lung cancer [8-11]. Since ICC contains a large proportion of non-tumor components [12], sequencing tumor sample directly may be confounded by low tumor purity, resulting in unexpected impacts on the accuracy of mutation landscape and clonal structure. As a countermeasure, PDPCs obtained by single sampling were developed for their high purity and cell population representativeness[13]. Previous study on hepatocellular carcinoma and lung cancer have shown that PDPCs can be an accurate assessment of intratumor genetic heterogeneity and represent a potential powerful tool for drug screening[13-15].

To reconstruct the genome history and evaluate how clonal structure can affect therapeutic responses in ICC, we performed multiregional WES of 6 ICC tumors containing a total of 69 related PDPCs that represented the broad intratumor mutational spectrum. The multiregional cell culture model derived from geographical sampling allowed us to study mutation frequencies, observe clonal evolution, and correlate evolution process with therapy development for ICC.

Method:

Patients and Sample Collection

Samples were collected from patients diagnosed with ICC who underwent curative resection without any adjuvant therapy before. All 6 patients were from Zhongshan Hospital of Fudan University. Patents' clinicopathologic information was presented in Supplementary Table 1. After resection, characteristic spatially separated regions of each primary tumor were collected as previously described[15]. Major part of each region was subjected to primary culture, and minor part was sent to H&E staining. Details of the establishment of PDPCs are described in the Supplementary Material. The study was approved by the Research Ethics Committee of Zhongshan Hospital, and written informed consent was obtained from each patient.

WES, Sanger validation, Fluorescent in situ hybridization, Immunohistochemistry, Cell proliferation assays, Genome-wide analysis of mutation calling, copy number alteration (CNA) and phylogenetic tree construction, and Statistical analysis.

see Supplementary Materials and Methods sections.

RESULTS

Establishment of multiregional patient-derived primary cancer cells from ICC

To illustrate ITH in ICC, fresh tissues were collected from 69 spatially distinct tumor regions (range, 7–16 per case) in 6 cases, who received curative resection (Supplementary Table 1). In particular, ICC1239P and ICC1239R were resected from the same patient, the latter of which was a recurrent lesion after 7 months of primary resection. Each sample was subjected to low-passage primary culture to generate PDPCs, followed by STR typing identification and WES (Graphical abstract). WES achieved a mean coverage of 100X on those 69 low-passage PDPCs and matched peripheral blood samples, as well as 300X on the corresponding tumor tissues (Supplementary Table 2).

As the low-passage primary culture would filter out most of the non-proliferative stromal components, the average purity of PDPCs finally achieved 94.4%(range, 67%-98%), compared to 40%(range, 20%-54%) in the tumor tissues(Supplementary Figure 1A). Thus, the high purity of PDPCs could minimize the confounding effect of non-tumor components on genomic analysis and was more conducive to build a model close to the real clonal structure[16]. Moreover, in each patient, the number of mutations detected in multiple PDPCs was significantly higher than that in its corresponding tissue (median, 832 vs 312) , while the mutations detected in the tissue with 300X sequencing depth was higher than those detected in any single PDPC with 100X depth (Supplementary Figure 1B), indicating that both multi-regional sampling and higher sequencing depth could improve the efficiency of mutation

detection. In addition, consistent with previous studies [13,15], there existed a similar mutation spectrum and mutation types between PDPCs and corresponding tissues. Altogether, multi-regional PDPCs could cover the whole mutation landscape and clonal structure more efficiently.

Spatial intratumor heterogeneity and clonal status of SNV

We identified a total of 1,596 non-silent mutations, including 1,312 missenses, 85 nonsenses, 25 splice-site variants and 174 insertions or deletions in those 69 PDPCs. Sanger validation of 1,331 randomly selected non-silent somatic mutations showed a high true discovery rate (94.4%) (Supplementary Table 4). Median number of non-silent mutations was 93 in each PDPCs and regions from same patients had similar numbers of mutations (Figure 1A, Supplementary Figure 2 and Supplementary Table 3). We found a high degree of spatial ITH in ICC. The median ITH index (Supplementary Method) is 60.3% (range 45.6%-71.6%), which is substantially higher than other cancers, such as esophageal adenocarcinoma (25%), non-small cell lung cancer (30%) and hepatocellular carcinoma (39%) [9,15,17]. In addition, we found that the genetic variability increased linearly with the number of sampling regions[18], showing that more regions were needed to accurately estimate the ITH level (Figure 1B).

For each individual region, we calculated the cancer cell fraction (CCF) and classified the mutations as clonal or subclonal using Pyclone[19]. Notably, almost a half of mutations (median 42.8%, range 8.3% to 79.4%) were classified as subclonal, implying that each individual region had high level of heterogeneity (Figure 1C, Supplementary Figure 3). The proportion of subclonal mutations in the regions was

higher than that of the cancers previously reported based on the TCGA data, such as bladder cancer (~18%), glioblastoma (~32%) and lung adenocarcinoma (~30%)[20]. Remarkably, duo to great variations in some given variant allele frequency among regions, a number of variants detected as clonal within some tumor regions were subclonal or absent in other regions from the same patients, producing an "illusion" of clonal dominance[9,21], and these clonal illusion mutations were detected in nearly all regions (Figure 1D). For instance, in ICC892, a missense mutation in KDM3A (pAla776Val), a member of the Jumonji C-domain-containing histone demethylases involved in cisplatin-resistance in ovarian cancer and tamoxifen-resistance in breast cancer[22,23], was estimated to be clonal in regions R2, R3 and R8 but was subclonal in all other 8 regions (Figure 1E). In fact, without multiregional WES, nearly 8% of subclonal mutations would be misinterpreted as clonal events. This misinterpretation may have serious adverse influence on the targeted therapy if only one region was used for sequencing analysis.

Tumor evolution of ICC

We further used Pyclone to construct phylogenetic tree to elucidate the evolutionary trajectory of each patient[19] (Figure 2A). On the phylogenetic trees, each cluster represented a node and the branch length was proportional to the mutation numbers in the corresponding cluster. In each patient, the trunk cluster consisted of clonal mutations and occured at early tumor stage. The trunk mutations formed the mutational profile of the founder population, representing optimal therapeutic targets. All the 6 patients displayed clear evidence of branched evolution. About half of the tumor regions (35/69, 50.2%) carried subclones located in only a single branch of the phylogenetic tree, once again demonstrating a high level of heterogeneity. The trunk

cluster of other cancer types often held the majority of the driver genes [9,17,24]. However, the driver genes in ICC were scattered along the phylogenetic tree, with only a minority located in the trunk. On average, trunk had only 4.3(15%) driver mutations and non-trunk had 24.7(85%) driver mutations. This indicated that the force to drive tumor diversity persisted along ICC evolution (Figure 2B). Considering the heterogeneity and the complex regulating network in ICC development[4,5,25], we clustered non-truncal missense genes into multiple pathways using the KEGG database, which exhibited that cAMP signaling, Calcium signal, cGMP-PKG signal, Gap junction and ECM-receptor pathways may have a crucial role in ICC progression (Figure 2C). We also adapted a dN/dS model to quantify the selection pressure in the tree. Although these data were still limited, dN/dS~1 appeared to characterize somatic evolution in ICC, while the ratio in missense mutations was higher than that in nonsense mutations (Wilcoxon test, p=0.006) (Supplementary Figure 4).

The same patient could have different and seemingly functional redundant mutations in the same driver gene. This is consistent with the parallel evolution that the same genetic pathway within a tumor was independently destroyed in different tumor subpopulations[26]. For example, in ICC772, two separate subclonal lineages, R3 and R7, carried different USP6 driver mutations that may activate USP6 oncogenic function and affect the Wnt signaling individually[27] (Figure 2E). Meanwhile, previous studies revealed that parallel evolution might also be driven by focal amplification[9,28]. In ICC892, the gene SMARCB1, a chromatin remodeler gene, had a trunk amplification, but they were further amplified in subclonal clusters and finally resulted in copy number hyper-diversity in the tumor sub-regions. These amplifications were validated by fluorescent in situ hybridization(FISH) analysis, using 2 probes labeling SMARCB1 (green) and 22q12 (red) respectively (Figure 2F).

Interestingly, the amplified alleles were always the SMARCB1-mutated (p.Arg367Met) allele.

When chromosome damage persisted, the expression of SMARCB1 might be up-regulated by multiple mechanisms, such as amplification, transcriptional and post-transcriptional regulation, while loss-of-function mutation in this gene may have interference in actual effect of amplification. Therefore, high expression of SMARCB1 mainly reflected the high level of chromosomal instability (CIN) and might be related with ICC prognosis. Immunostaining showed a typical nuclear staining of SMARCB1 in ICC, and 63% (197/311) of patients displayed up-regulation of SMARCB1[25] (Figure 2G). SMARCB1 expression was independent of patients' clinicopathologic characteristics(Supplementary Table 5), and its high expression significantly correlated with dismal clinical outcome (Figure 2H). Multivariate analysis also confirmed SMARCB1 expression as an independent prognosticator for recurrence (hazard ratio [HR], 1.37; 95% confidence interval [CI], 1.01–1.85; P= 0.043) and survival(HR, 1.59; CI, 1.19-2.97; p=0.002) (Supplementary Tables 6 and 7).

Temporal dissection of mutational spectrum and signatures

We further analyzed the mutational spectrum based on the timeline of mutation acquisition, i.e., early trunk, late trunk and non-trunk mutations. Among all mutations, C>A transversion, C>T and T>C transitions were the predominant changes, a feature shared by hepatocellular carcinoma and ICCs[29]. Similar to previous reports in ICC [5,6], the C>T transitions in our 6 ICCs were enriched in CpG sites, implying a common mechanism underlying ICC pathogenesis. In addition, C>A transversion

increased dramatically in non-trunk mutations, while the proportion of T>C transition decreased in non-trunk (Figure 3A and 3B).

To figure out the cause of such mutation shift, we analyzed the mutation signatures using DeconstructSigs to map the mutation to the COSMIC signatures[30](Figure 6a). The signatures in the trunk and non-trunk mutation demonstrated significant differences. Correspondending to the change of C>A transversion, signature 24, observed in a subset of hepatocellular carcinoma that correlated with aflatoxin B exposure, displayed a prominent increase only in non-trunk events, especially in ICC880 and ICC1969. Additionally, the tobacco-related signature 29 was elevated in non-trunk events, consistent with the smoking history of these patients. Moreover, signature 5 was increased in 4 ICC patients, but the etiology of this signature was still unknown. These ICCs could acquire different branched driver genes with similar mutation signatures, indicating the innate essence rather than the mutation signatures may be the predominant fuel for branch process(Figure 3C).

The distribution of signatures in the trunk was more diversified than that in the non-trunk (Figure 3C), implying that complicated etiology may be involved in the tumorigenesis of different individuals. Signature 1, reflecting spontaneous deamination of methylated cytosines, was identified in ICC880 and ICC1969 and was significantly more prevalent in the trunk mutation. This signature was associated with ICC patient age at diagnosis, indicating these initial mutations may accumulate with age. Another tobacco-related signature, signature 4, was found in the trunk, indicating that effect of tobacco consumption will affect the entire evolution process. Signature 16 was also found to be elevated in the trunk mutation. Signature 16 was linked with an exceptionally strong transcriptional strand bias for T>C mutations at ApTpN context but its etiology was still unknown.

The heterogeneity of CNA and chromosomal instability

We next analyzed heterogeneity at the copy number level. In contrast to high degree of ITH in somatic mutations, CNAs showed less degree of intra-tumor heterogeneity. We detected deletions on chromosomes 1p, 4q, 7q, 8p, 13q, 16q and 22q (deletion: <=1 copy number relative to ploidy). These deletions harbored well-known tumor suppressors, such as TP53 (17p13), RB1 (13q13) and ARID1A (1p36). ARID1A was identified as an ICC driver in previous genomic sequencing studies[5,6], and its inactivation was proved to promote ICC carcinogenesis[5]. We also noted high level of amplification on chromosomes 6p, 7p, 8q, 9q and 12p, 22q (amplification: >= 2X ploidy). Known oncogenes, such as EGFR, CDK6, MET, MYC, HOXA9, and SALL4, were located in these regions (Figure 4A). Circos plot of 6 patients were also drawn to present the CNA profiles (Supplementary Figure 5). In addition, the somatic CNAs in our cohort were compared with those in another 99 ICC patients using an in-house algorithm based on BICseq2 and GISTIC2.0[6,31,32]. In total, 30 amplified segments and 20 loss segments also existed in at least one sample in our cohort, indicating a significant overlap with this dataset (Figure 4B). Deletions of both TP53 and ARID1A were found in half of ICCs (50/99), and high frequent amplification of the above oncogenes were also observed.

Remarkably, except for ICC1239 (diploid), the remaining 5 cases held high-ploidy karyotypes. ICC772, ICC 892, ICC1370 and ICC1969 were triploid and ICC 880 was tetraploid(Figure 4A). The allele information of these high-ploidy tumors showed that genome doubling (GD) was shared by all regions and hence GD would be an early event in tumor progression. All the high-ploidy patients held the deletion of 17p, where the tumor suppressor gene TP53 located. Increasingly more evidences indicted

that GD events were associated with increased CIN and may forecast poor prognosis[33]. Previous study showed that a 20% threshold of the weighted Genome Instability Index (wGII) could accurately distinguish CIN+ from CIN− tumors[34]. We found that all tumor regions in our cohort demonstrated high levels of wGII (median, 0.67; range, 0.31–0.93), indicative of CIN+. Considerably higher wGIIs were detected in high-ploid (ploidy ≥3) than diploid tumors, consistent with the results in colorectal cancer[33](Figure 4C). Alternatively, studies reported that microsatellite instability existed in some ICC with a more favorable outcome and could predict the response to PD-1blockade [35,36]. However, samples in this cohort showed very low MSI scores (Supplementary Figure 6). These data conformed with the model that extensive CIN occurred along with the evolution and provided sufficient fuel for clonal diversification in ICC.

Timing of Clonal mutations and chromosomal alterations

Alterations in a number of driver genes were mostly truncal and occurred before GD, indicating their involvement in tumor initiation. For instance, other than SMARCB1, several other SWI/SNF complex gene, including SS18, PBRM1 and SMARCC1, also harbored clonal inactivating mutations in 4/6 cases, and most of them occurred before GD. In our 5 high-ploidy ICCs, GD was found to mainly occur later in the trunk, resulting in mutated allele copy number ≥2 for most of truncal mutations (median 83%, range, 78-89%). In other word, a significant mutational burden had already accumulated before GD in ICC.

Clonal chromosomal-arm alterations were further timed by mutated allele copy number of all genes on a given arm. In the 5 ICC, early alterations were estimated to

include the amplifications of 6p, 7p and 12p and the LOH of 1p, 8p, 13q and 22q12 before GD. For example, 22q12 LOH (2+0), harboring the tumor suppressor NF2, was likely to have occurred prior to GD and promote the initiation of ICC892; Otherwise, it would require two independent hits. The copy number of 22q12 was validated by FISH analysis in regions R3, R8 and R9(Figure 2F, the red spot).

Intrahepatic metastasis and polyclonal seeding

Next, we assessed the temporal association between the primary and recurrent lesions in ICC1239. Considering that both of them shared the same clonal mutations and similar mutation spectrum, we inferred that ICC1239R was formed by the early intrahepatic metastasis from the primary tumor ICC1239P, rather than a new multi-centric tumor(Figure 5A). If a recurrence was seeded by single tumor cell, it should carry a series of alterations that presented in all tumor cells. However, in ICC1239R, multiple mutational clusters presented subclonally in more than one recurrent region. The recurrence would thus most likely come from multiple seeding by two or more distinct primary clusters, indicative of polyclonal metastatic seeding in ICC (Figure 6B and 6C). The multiple seeding events could be attributed to two factors: first, a cooperative relationship existed among these clusters; second, early colonization was actively involved in remodeling local microenvironment to make it conducive to later colonization. Consistently, recent studies revealed subclonal reciprocal interaction through Wnt and Notch pathways to promote cancer metastasis[37,38].

Moreover, ICC1239R had an equal number of clonal mutations but much fewer subclonal mutations compared to ICC1230P (Supplementary Figure 4). Many subclonal mutations in primary site, such as mutations in the genes KIAA0232 and

IGF2BP3, could not be detected in the recurrence. This was consistent with the "founder effect" theory that the diversity of genome alteration in the metastases was much less than primary tumor[39,40](Figure 5B and 5C). In addition, new oncogenic events occurring during metastatic progression would endow the recurrence with a new phenotype. Although ICC were highly chemoresistant tumor, genetic alterations related to chemoresistance would make ICC1239R respond differently to chemotherapy. For example, a nonsilent mutation in PFKP (p.Ile752Leu), a gene that potentiated cancer cell survival under metabolic stress and mediated resistance to cisplatin in ovarian cancer[41], was clonal in the region ICC1239R_R2, but undetectable in all other primary or recurrent regions. Additionally, two chemoresistance-related genes in ICC1239R_R2 exhibited copy-number loss. One was a nucleotide excision repair gene ERCC2. Its deficiency would contribute to cisplatin sensitivity in urothelial cancer and non-small cell lung cancer[42,43]. The other was AKT-2. The loss of AKT-2 could lead to apoptosis via Bcl-2 downregulation and Bax upregulation, and sensitize cells to cisplatin[44]. Therefore, we tested the effect of cisplatin on cell viability of the primary cells derived from 1239R_R1/R2 in vitro, and the result was consistent with the genomic prediction(IC50 of R1 and R2: 11.3μmol/L and 3.5μmol/L respectively)(Figure 5D). These alterations thus indeed made ICC1239R_R2 more sensitive to cisplatin-based chemotherapy than other regions.

Potential target strategy for ICC treatment

We next considered all alterations with available or in-development therapeutics. To maximize tumor response, the most prior strategy was to target clonal events in all tumor cells. In 5/6 patients, there were actionable clonal truncal mutations (see

Supplementary Material). TP53 in ICC1370 and ICC880, SMARCB1 and RB1 in ICC892 were clonal in all the regions, but there were no FDA-approved drugs targeting these genes. ICC1239 had a truncal IDH1 mutation (p.Arg132Cys) and a JAK1 mutation (p.Tyr1059Cys). The IDH inhibitor AG-120 and JAK inhibitor Ruxolitinib might be used for these two mutations. ICC880 had a truncal KRAS mutation (p.Gly12Asp) and the patient may benefit from Panitumumab or combinational treatment of Cetuximab plus chemotherapy[45,46]. Except region R3, EGFR amplification were detected in all regions of ICC1969,, making them potentially sensitive to Gefitinib[47](Supplementary Figure 7). We selected Gefitinib, an EGFR inhibitor, to test its effect on cell viability of PDPCs from ICC1969 using ICC772 cells without EGFR alterations as a control. The results showed that EGFR amplification indeed made ICC1969 cells more susceptible to anti-EGFR therapy (Supplementary Figure 8).

Considering the clonal structure in the recurrence ICC1239R, adaptive therapy, an evolution-based therapeutic strategy that aimed to prolong time to progression rather than to reduce tumor size[48], would be optimal to control its progression. ICC1239_R2 was sensitive to cisplatin-based chemotherapy, and thus would cost fewer intracellular resources to maintain resistance and consequently have higher fitness than resistant cells when not treated [49](Figure 5E). In this model, the patient may be first given targeted trunk therapy, such as Ruxolitinib and AG-120, to dwindle the population of all clusters, followed by a non-treatment stage to allow the cell population with higher fitness (1239_R2) to expand and suppress the growth of chemo-resistant population. Next, a cisplatin-based chemotherapy in low and short burst dosage would be applied to kill most of the sensitive cells with little influence on resistant population and then be withdrawn. Gradually, the resistant population would be inhibited by the sensitive population and grow slowly and another round of

targeted trunk therapy could be initiated again when the resistant population did progress. Adaptive strategies like adjusting the conduction of the drug vacations and treatments targeting different tumor branches, in conjunction with medical imaging or liquid biopsy to monitor subclonal growth ratios, could stimulate clonal competition and restrain general tumor growth[50].

DISCUSSION

In this study, we depicted an overall picture of intratumor genetic heterogeneity and unmasked the evolutionary trajectories in ICC. Our results demonstrated that multiple evolutionary mechanisms, like branch evolution and parallel evolution of late mutations, “illusion” of clonal dominance and polyclonal metastatic seeding, had important roles in ICC progression. In addition to intrinsic genetic instability, we found that extrinsic factors, such as carcinogenic exposure, smoking history, aging and others, might collectively contribute to shape intratumor genetic heterogeneity of ICC. Notably, all the tumors in our cohort carried subclonal driver alterations, stressing the importance of spatial heterogeneity in ICC on fully capturing tumor evolutionary history and on more accurately identifying driver events as attractive therapeutic targets(Figure 6).

The evolution trajectory was constructed based on somatic alterations to reflect the history of ICC development, showing that branch evolution was the dominant pattern. In fact, several targetable driver mutations, including those in JAK1, IDH1, and KRAS, were almost exclusively truncal events, which could be optional targets for devising new therapies. However, over 85% of putative driver mutations, such as ERBB2, CTNNB1, NOTH1, HIF1A, TTN, KDM3A and IKZF1[5,6,51,52], were

found to be subclonal in these 6 ICCs. Furthermore, evidence of parallel evolution of branch alterations in both SNVs and CNAs was noted, and FISH-based analyses confirmed the heterogeneity of copy-number changes. These driver alterations in parallel branches were relatively late events during tumor evolution and represented the constraints imposed on cancer development. Therefore targeting parallel evolutionary events and exploiting these cancer dependencies may be a compelling approach. In a word, we can reasonably infer that the trunk mutations in ICC may just confer fundamental ability for tumorigenesis, while the non-truncal mutations preferentially favor distinct subclonal expansions after establishment of the founding clones.

Meanwhile, our study also provided information on the divergent chromosomal instability processes related to ICC evolution and their dynamics over time. GD events, a macro-evolutionary step in cancers[33], were observed in 5 out of 6 ICC patients. In all 5 patients, genome-doubling events were found to occur before subclonal diversification but after acquisition of most of early driver mutations, consistent with findings in colorectal and esophageal cancer that GD may accelerate cancer genome evolution[17,33]. Furthermore, we found that all tumor regions in our cohort demonstrated high levels of chromosomal instability index, along with mutations or deletions in specific genes involved in maintaining genome integrity and DNA repair, e.g. the chromatin remodeling complex. It is worth noting that truncal mutations can be lost by later copy-number deletion, which will restrict the potential of targeted truncal strategy, especially in tumors with high chromosomal instability. Consequently, these findings suggested that chromosomal instability was wide-spread in ICCs at both early and late stage and fueled for evolution process. As a potential therapeutic strategy, reduced genome instability may limit the ensuing heterogeneity and adaptability of cancer cells to treatments.

Interestingly, in ICC1239 with primary and intrahepatic metastatic tumors, the clear evidence of polyclonal metastatic seeding supported that tumors existed as symbiotic communities of multiple clones that were maintained during metastasis[53]. Despite intratumor heterogeneity, the truncal alterations were generally consistent between the primary and intrahepatic metastasis, indicating that multi-region sequencing of primary tumor could be adequate to find the targets in the trunk to deal with the metastasis. Meanwhile, genetic diversity of polyclonal populations could be greatly reduced in the metastasis by the "founder effect", with several newly-acquirred alterations. New alterations in 1239R_R2 made it more sensitive to the cisplatin than other recurrences, validated by in vitro drug test, which might provide a theoretical basis for adaptive therapy and showed a potential to evoke the competition between clonal subgroups in ICC.

Several limitations may undermine this study. First, although M-WES achieves more tumor diversity than single biopsy, the tissue it sampled is still limited. Hence, this approach still underestimates the number of subclones present within a given tumor, leading to limited resolution of the evolutionary trajectory. Conceivably, higher sequencing depth and integrated omics data, like epigenomics, transcriptomics and proteomics, may help to generate fine structure. Second, comparing to somatic mutations, detection of subclonal CNAs remains challenging, and significant subclonal amplifications or deletions may be ignored. Novel technologies, such as the third-generation sequencing, are needed to overcome the limitation. Third, therapeutic strategies proposed here need further validation in large-scale preclinical and clinical studies.

In summary, integrating PDPCs culture and multiregional WES, we revealed strong spatial, temporal ITH and diversity of clonal status, constructed the clonal evolution

trajectory in ICC, and marked the chromosomal instability as the main power source of evolution.

Acknowledgements

The authors are grateful to Dr. Yi-Hui Lin for help with PDPCs establishment, from Institute of Precision Medicine, 3D Medicines Inc., Shanghai, China

References

1. Fitzmaurice, C. et al. The Global Burden of Cancer 2013. *JAMA Oncol* **1**, 505–527 (2015).
2. Valle, J. *et al.* Cisplatin plus gemcitabine versus gemcitabine for biliary tract cancer. *N. Engl. J. Med.* **362,** 1273–1281 (2010).
3. Bridgewater, J. et al. Guidelines for the diagnosis and management of intrahepatic cholangiocarcinoma. *J. Hepatol*. **60**, 1268–1289 (2014).
4. Ong, C. K. *et al.* Exome sequencing of liver fluke-associated cholangiocarcinoma. *Nat. Genet.* **44,** 690–693 (2012).
5. Jiao, Y. *et al.* Exome sequencing identifies frequent inactivating mutations in BAP1, ARID1A and PBRM1 in intrahepatic cholangiocarcinomas. *Nat. Genet.* **45,** 1470–1473 (2013).
6. Zou, S. *et al.* Mutational landscape of intrahepatic cholangiocarcinoma. *Nat Commun.* **341,** 5696 (2014).
7. Shi, H. *et al.* Acquired resistance and clonal evolution in melanoma during BRAF inhibitor therapy. *Cancer Discov* **4,** 80–93 (2014).
8. Gundem, G. *et al.* The evolutionary history of lethal metastatic prostate cancer. *Nature* **520,** 353–357 (2015).
9. Jamal-Hanjani, M. *et al.* Tracking the Evolution of Non-Small-Cell Lung Cancer. *N. Engl. J. Med.* **376,** 2109–2121 (2017).
10. Shi, J.-Y. *et al.* Inferring the progression of multifocal liver cancer from spatial and temporal genomic heterogeneity. *Oncotarget* **7,** 2867–2877 (2016).
11. Duan, M. *et al.* Diverse modes of clonal evolution in HBV-related hepatocellular carcinoma revealed by single-cell genome sequencing. *Cell Res.* **65,** 87 (2018).

12. Rizvi, S. & Gores, G. J. Pathogenesis, Diagnosis, and Management of Cholangiocarcinoma. *Gastroenterology* **145,** 1215–1229 (2013).

13. Crystal, A. S. *et al.* Patient-derived models of acquired resistance can identify effective drug combinations for cancer. *Science* **346,** 1480–1486 (2014).

14. Bissig-Choisat, B. *et al.* Novel patient-derived xenograft and cell line models for therapeutic testing of pediatric liver cancer. *J. Hepatol.* **65,** 325–333 (2016).

15. Gao, Q. *et al.* Cell Culture System for Analysis of Genetic Heterogeneity Within Hepatocellular Carcinomas and Response to Pharmacologic Agents. *Gastroenterology* **152,** 232–242.e4 (2017).

13. Aran, D., Sirota, M. & Butte, A. J. Systematic pan-cancer analysis of tumour purity. *Nat. Commun.* **6,** 8971 (2015).

17. Murugaesu, N. *et al.* Tracking the genomic evolution of esophageal adenocarcinoma through neoadjuvant chemotherapy. *Cancer Discov* **5,** 821–831 (2015).

15. Zhai, W. *et al.* The spatial organization of intra-tumour heterogeneity and evolutionary trajectories of metastases in hepatocellular carcinoma. *Nat. Commun.* **8,** 4565 (2017).

19. Roth, A. *et al.* PyClone: statistical inference of clonal population structure in cancer. *Nat. Methods* **11,** 396–398 (2014).

20. McGranahan, N. *et al.* Clonal status of actionable driver events and the timing of mutational processes in cancer evolution. *Sci Transl Med* **7,** 283ra54–283ra54 (2015).

21. Gerlinger, M. *et al.* Intratumor heterogeneity and branched evolution revealed by multiregion sequencing. *N. Engl. J. Med.* **366,** 883–892 (2012).

22. Mahajan, K., Bandyopadhyay, S. & Mahajan, N. Abstract 2599: KDM3A

tyrosine phosphorylation by Ack1 promotes tamoxifen-resistance in breast cancer. *Cancer Res.* **74,** 2599–2599 (2014).

23. Ramadoss, S., Sen, S., Chaudhuri, G. & Farias-Eisner, R. Abstract 5143: KDM3A promotes cell growth and cisplatin-resistance in ovarian cancer cells. *Cancer Res.* **74,** 5143–5143 (2014).
24. Torrecilla, S. *et al.* Trunk mutational events present minimal intra- and inter-tumoral heterogeneity in hepatocellular carcinoma. *J. Hepatol.* **67,** 1222–1231 (2017).
25. Gao, Q. *et al.* Activating mutations in PTPN3 promote cholangiocarcinoma cell proliferation and migration and are associated with tumor recurrence in patients. *Gastroenterology* **146,** 1397–1407 (2014).
26. Gerlinger, M. *et al.* Genomic architecture and evolution of clear cell renal cell carcinomas defined by multiregion sequencing. *Nat Genet* **46,** 225–233 (2014).
27. Madan, B. *et al.* USP6 oncogene promotes Wnt signaling by deubiquitylating Frizzleds. *Proc. Natl. Acad. Sci. U.S.A.* **113,** E2945–54 (2016).
28. Yates, L. R. *et al.* Subclonal diversification of primary breast cancer revealed by multiregion sequencing. *Nat. Med.* **21,** 751–759 (2015).
29. Alexandrov, L. B. *et al.* Signatures of mutational processes in human cancer. *Nature* **500,** 415–421 (2013).
30. Rosenthal, R., McGranahan, N., Herrero, J., Taylor, B. S. & Swanton, C. DeconstructSigs: delineating mutational processes in single tumors distinguishes DNA repair deficiencies and patterns of carcinoma evolution. *Genome Biol.* **17,** 31 (2016).
31. Mermel, C. H. *et al.* GISTIC2.0 facilitates sensitive and confident localization of the targets of focal somatic copy-number alteration in human cancers. *Genome Biol.* **12,** R41 (2011).

32. Xi, R., Lee, S., Xia, Y., Kim, T.-M. & Park, P. J. Copy number analysis of whole-genome data using BIC-seq2 and its application to detection of cancer susceptibility variants. *Nucleic Acids Res.* **44,** 6274–6286 (2016).

33. Dewhurst, S. M. *et al.* Tolerance of Whole-Genome Doubling Propagates Chromosomal Instability and Accelerates Cancer Genome Evolution. *Cancer Discov* **4,** 175–185 (2014).

34. Lee, A. J. X. *et al.* Chromosomal instability confers intrinsic multidrug resistance. *Cancer Res.* **71,** 1858–1870 (2011).

35. Cloyd, J. M. *et al.* Long-Term Survival Among Mismatch Repair Deficient Cholangiocarcinomas Associated with Lynch Syndrome. *Gastroenterology* **152,** S1254 (2017).

36. Le, D. T. *et al.* Mismatch repair deficiency predicts response of solid tumors to PD-1 blockade. *Science* **357,** 409–413 (2017).

37. Tammela, T. *et al.* A Wnt-producing niche drives proliferative potential and progression in lung adenocarcinoma. *Nature* **545,** 355–359 (2017).

38. Lim, J. S. *et al.* Intratumoural heterogeneity generated by Notch signalling promotes small-cell lung cancer. *Nature* **545,** 360–364 (2017).

39. Wu, X. *et al.* Clonal selection drives genetic divergence of metastatic medulloblastoma. *Nature* **482,** 529–533 (2012).

40. Johnson, B. E. *et al.* Mutational analysis reveals the origin and therapy-driven evolution of recurrent glioma. *Science* **343,** 189–193 (2014).

41. Kim, N. H. *et al.* Snail reprograms glucose metabolism by repressing phosphofructokinase PFKP allowing cancer cell survival under metabolic stress. *Nat. Commun.* **8,** 14374 (2017).

42. Van Allen, E. M. *et al.* Somatic ERCC2 mutations correlate with cisplatin

sensitivity in muscle-invasive urothelial carcinoma. *Cancer Discov* **4,** 1140–1153 (2014).

43. Olaussen, K. A. *et al.* DNA Repair by ERCC1 in Non–Small-Cell Lung Cancer and Cisplatin-Based Adjuvant Chemotherapy. *N. Engl. J. Med.* **355,** 983–991 (2006).
44. Yoon, H., Min, J.-K., Lee, J. W., Kim, D.-G. & Hong, H. J. Acquisition of chemoresistance in intrahepatic cholangiocarcinoma cells by activation of AKT and extracellular signal-regulated kinase (ERK)1/2. *Biochem. Biophys. Res. Commun.* **405,** 333–337 (2011).
45. Douillard, J.-Y. *et al.* Randomized, phase III trial of panitumumab with infusional fluorouracil, leucovorin, and oxaliplatin (FOLFOX4) versus FOLFOX4 alone as first-line treatment in patients with previously untreated metastatic colorectal cancer: the PRIME study. *J. Clin. Oncol.* **28,** 4697–4705 (2010).
46. De Roock, W. *et al.* Effects of KRAS, BRAF, NRAS, and PIK3CA mutations on the efficacy of cetuximab plus chemotherapy in chemotherapy-refractory metastatic colorectal cancer: a retrospective consortium analysis. *Lancet Oncol.* **11,** 753–762 (2010).
47. Petty, R. D. *et al.* Gefitinib and EGFRGene Copy Number Aberrations in Esophageal Cancer. *J. Clin. Oncol.* **35,** 2279–2287 (2017).
48. Enriquez-Navas, P. M. *et al.* Exploiting evolutionary principles to prolong tumor control in preclinical models of breast cancer. *Sci Transl Med* **8,** 327ra24–327ra24 (2016).
49. West, J., Ma, Y. & Newton, P. K. Capitalizing on Competition: An Evolutionary Model of Competitive Release in Metastatic Castrate Resistant Prostate Cancer Treatment. *bioRxiv*, 190140(2017)

50. Amirouchene-Angelozzi, N., Swanton, C. & Bardelli, A. Tumor Evolution as a Therapeutic Target. *Cancer Discov* **7,** 805–817 (2017).

51. Sia, D. *et al.* Integrative molecular analysis of intrahepatic cholangiocarcinoma reveals 2 classes that have different outcomes. *Gastroenterology* **144,** 829–840 (2013).

52. Sia, D. *et al.* Massive parallel sequencing uncovers actionable FGFR2-PPHLN1 fusion and ARAF mutations in intrahepatic cholangiocarcinoma. *Nat. Commun.* **6,** 6087 (2015).

53. Speicher, M. R. Searching for cancer vulnerabilities amid genetic chaos. *Genome Biol.* **18,** 147 (2017).

Figure legends

Figure 1: Intratumor genetic heterogeneity of ICC. **(A)** Number of somatic SNVs and the distribution of different mutation types. (**B)** The relationship between detected genetic variability and the number of samples acquired within a tumor. (**C)** The distribution of CCF 95%CI among all mutations. This plot includes the mutations with <5% CCF, which have been excluded for further analysis. (**D)** Barplot shows all subclonal mutations, and it will be counted as clonal illusion (blue) if one appears clonal in at least one region. (**E)** Representative probability distributions over the CCF of KDM3A in ICC892.

Figure 2: Phylogenetic tree and parallel evolution. **(A)** Coxcomb plots presenting the clinical information and ITH parameters(upper panel) and reconstruction of phylogenetic trees in the 6 cases(lower panel). (**B)** The distribution of driver genes in the trunk and non-trunk. (**C)** The main pathways involved in the non-trunk alterations, referring to the KEGG database. (**D)** Parallel evolution in ICC772 driven by two different USP6 mutations. (**E)** Parallel evolution of amplification of SMARCB1 in ICC892. The copy number of SMARCB1 progresses step by step, validated by FISH analysis. (**F)** Representative immunostaining images of SMARCB1 protein in normal liver tissue and ICC. Samples with scores 0 and 1 are divided into $SMARCB1^{low}$ group, and scores 2 and 3 into $SMARCB1^{high}$ group. Scale bars=100um. **(G)**. Kaplan-Meier curves showing increased recurrence and dismal survival in patients of $SMARCB1^{high}$ group.

Figure 3: Temporal dissection of mutational process and signatures in ICCs **(A)** The 96 trinucleotide mutational spectra of trunk (right) and non-trunk (left) mutations. (**B)** Proportion of 4 distinct mutation types is shown for trunk and non-trunk mutations. (**C)** Dot plots showing the distribution of mutation signature to each patient in trunk and non-trunk(left) and pie charts indicating signature distributions (right).

Figure 4: Heterogeneity of CNV and chromosomal instability. **(A)** Heatmap of copy number variants. X-axis shows chromosomal coordinates. The right band displays the ploidy status. (**B)** The significance of focal somatic CNAs in 99 ICCs. GISTIC q-values (x-axis) for deletions (right, blue) and amplifications (left, red) are plotted across the genome (y-axis). Known or putative gene targets within the peak regions are indicated. (**C)** The correlation of the ploidy and wGII. Positive correlation between the ploidy and wGII is observed and all regions have evidence of CIN.

Figure 5: Polyclonal seeding and adaptive therapy **(A)** A timeline of clinical history in ICC1239P and ICC1239R. Representative CT/MRI images of each tumor are shown below and the red circles indicate the locations of tumors. **(B)** The brief diagram of phylogenetic tree. The orange branch and grey branch represent the ICC1239R and ICC1239P, respectively. (**C)** CCF comparisons for the primary and recurrent regions. In the plot, the CCF of all SNVs for all primary sites (y-axis) is plotted against the 3 recurrent sites (x-axis). (**D)** The viable test of cisplatin treatment of PDPCs from R1/R2. P=0.008. (**E)** Fitness landscape with and

without chemotherapy[left] and a model based on adaptive therapy which may be suitable for ICC1239R to prolong patient survival time[right].

Figure 6: A model of the evolutionary history of ICC. ICC evolves through acquisition of driver genes. Lots of mechanisms are involved in branch diversity, which is collectively shaped by positive selection, parallel evolution and chromosome instability. GD: genome doubling; LOH loss of heterogeneity.

Highlights

- Branch evolution is the predominant pattern in ICC, which is collectively shaped by parallel evolution and chromosome instability.
- ICC may metastasize through polyclonal seeding and the competition between subclonal population can be used to develop new treatment strategy, like adaptive therapy.
- Targeted therapy against truncal alterations, such as IDH1, JAK1, and KRAS mutations and EGFR amplification, can be a promising treatment strategy for ICC patients.

Figure 1

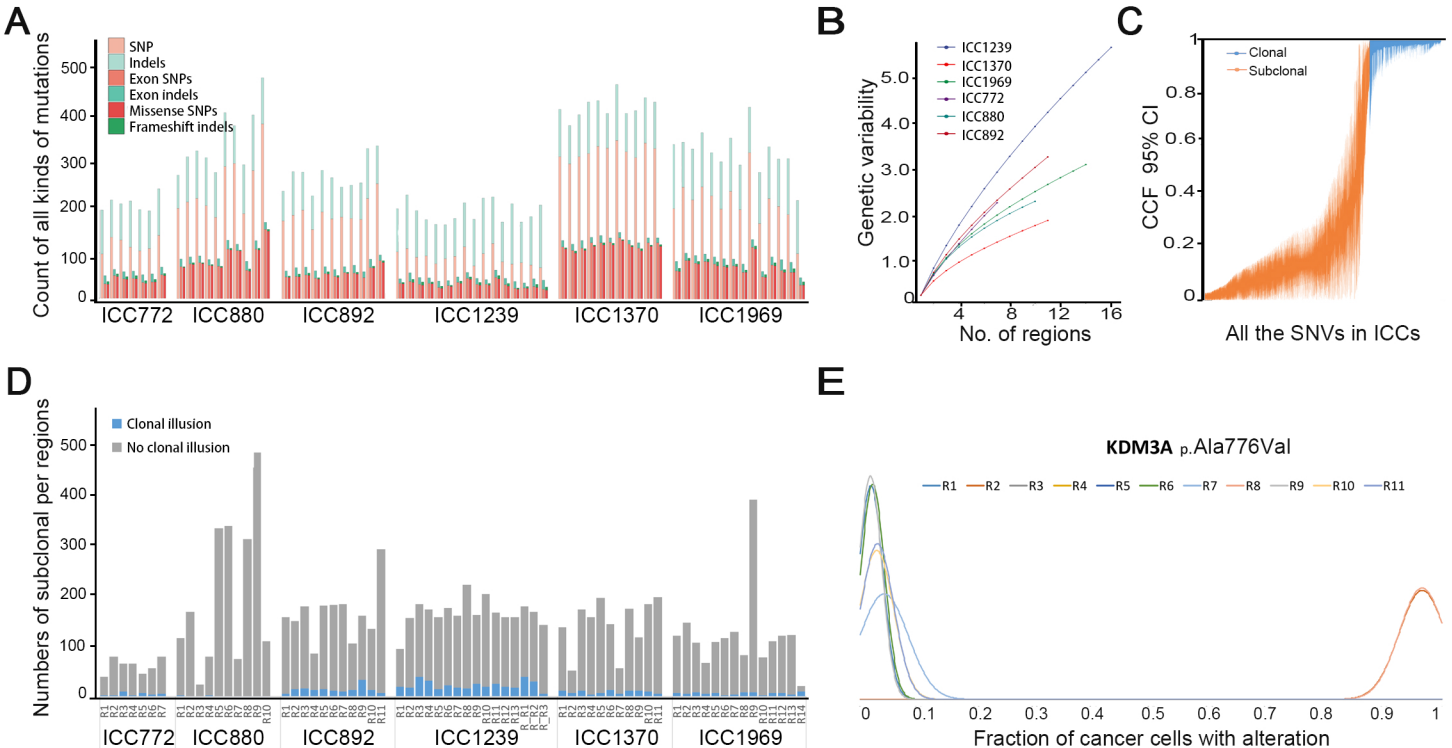
A
Count of all kinds of mutations
SNP
Indels
Exon SNPs
Exon indels
Missense SNPs
Frameshift indels
ICC772
ICC880
ICC892
ICC1239
ICC1370
ICC1969
B
Genetic variability
No. of regions
ICC1239
ICC1370
ICC1969
ICC772
ICC880
ICC892
C
CCF 95% CI
Clonal
Subclonal
All the SNVs in ICCs
D
Numbers of subclonal per regions
Clonal illusion
No clonal illusion
ICC772
ICC880
ICC892
ICC1239
ICC1370
ICC1969
E
KDM3A p.Ala776Val
Fraction of cancer cells with alteration

Figure 2

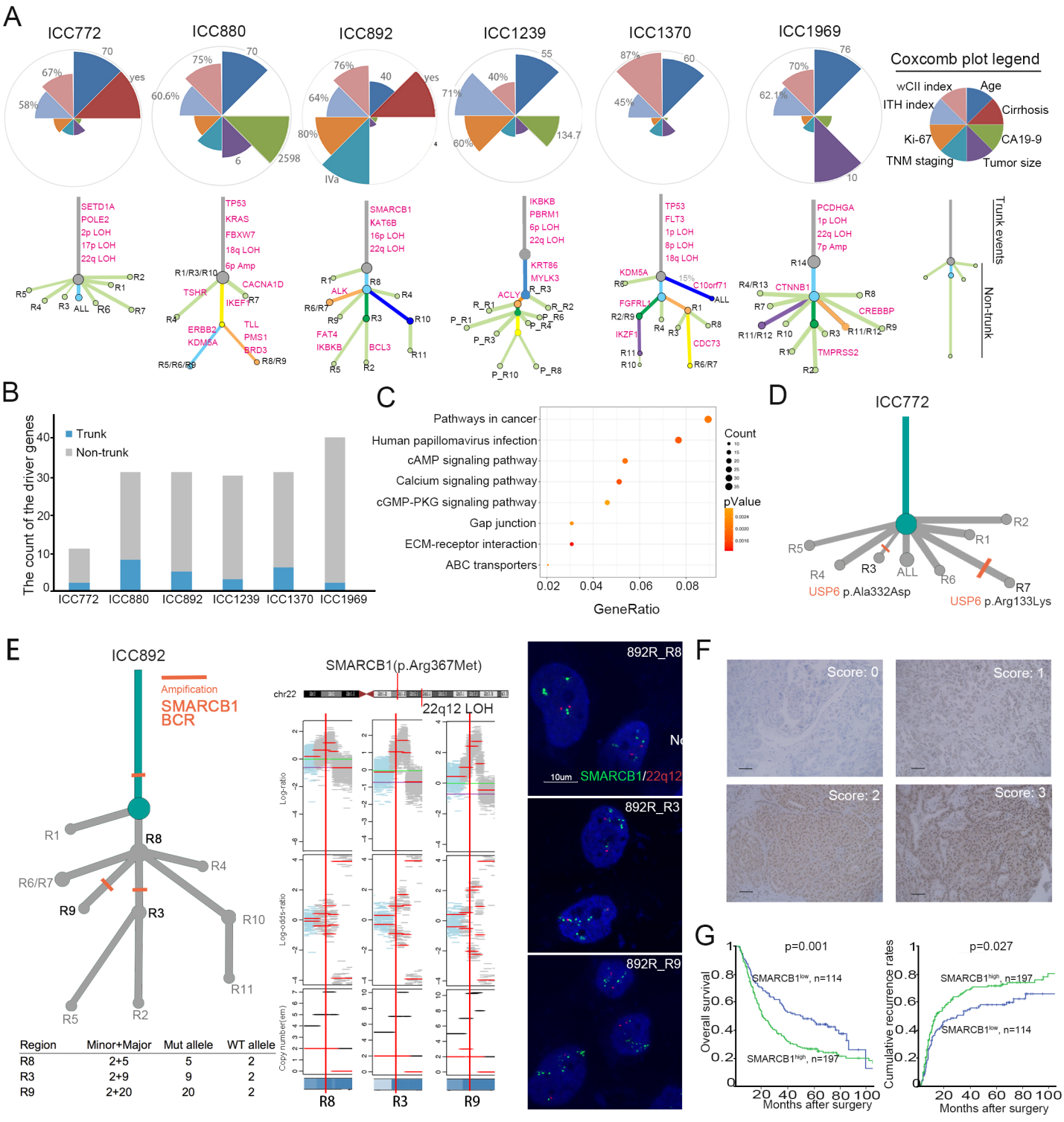

Region	Minor+Major	Mut allele	WT allele
R8	2+5	5	2
R3	2+9	9	2
R9	2+20	20	2

Figure 3

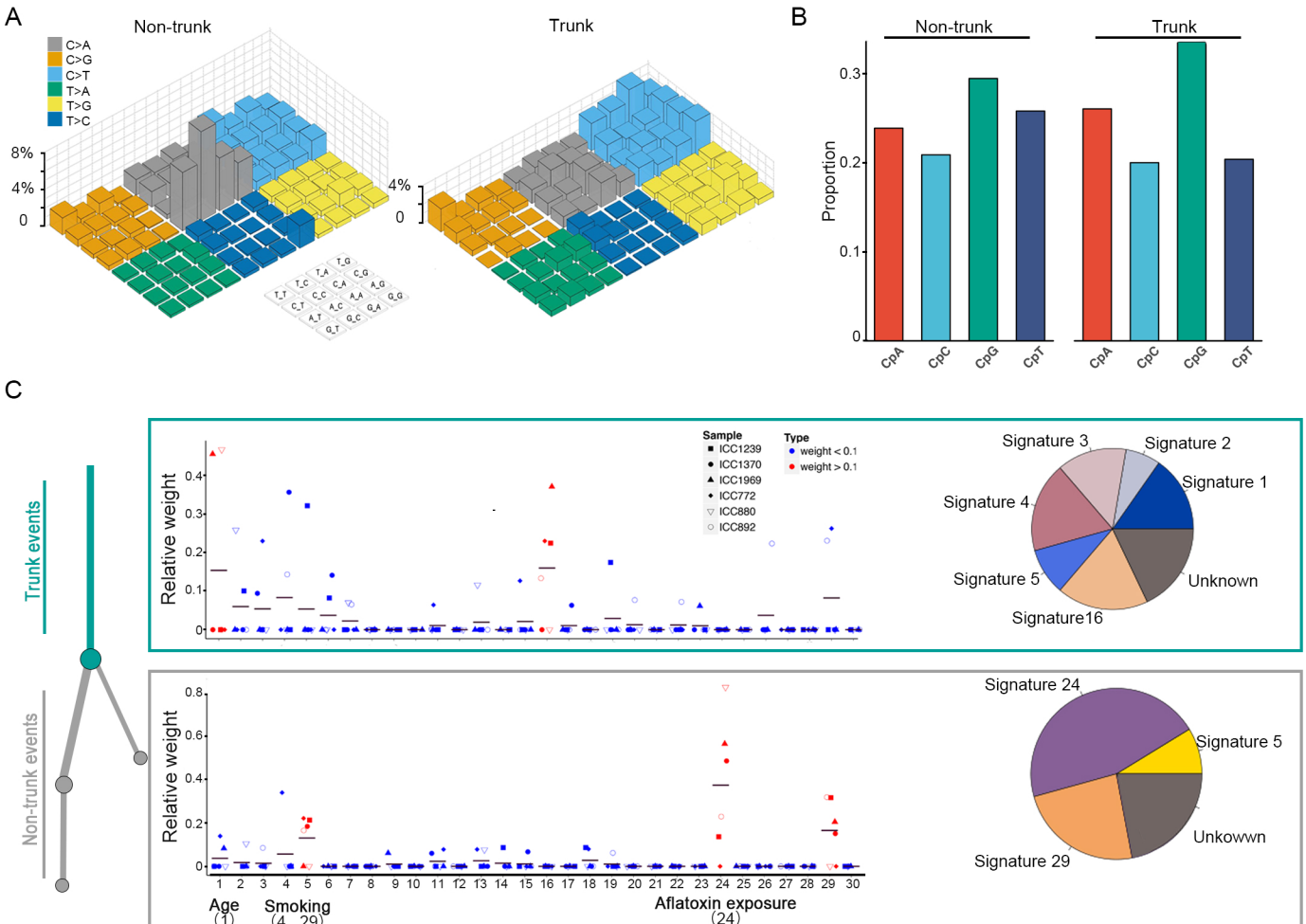
A
Non-trunk
Trunk
C>A
C>G
C>T
T>A
T>G
T>C
8%
4%
0
4%
0
B
Non-trunk
Trunk
Proportion
0.3
0.2
0.1
0
CpA
CpC
CpG
CpT
C
Trunk events
Non-trunk events
Relative weight
Sample
ICC1239
ICC1370
ICC1969
ICC772
ICC880
ICC892
Type
weight < 0.1
weight > 0.1
Signature 3
Signature 2
Signature 1
Signature 4
Signature 5
Unknown
Signature16
Relative weight
Age
(1)
Smoking
(4,, 29)
Aflatoxin exposure
(24)
Signature 24
Signature 5
Unkowwn
Signature 29

Figure 4

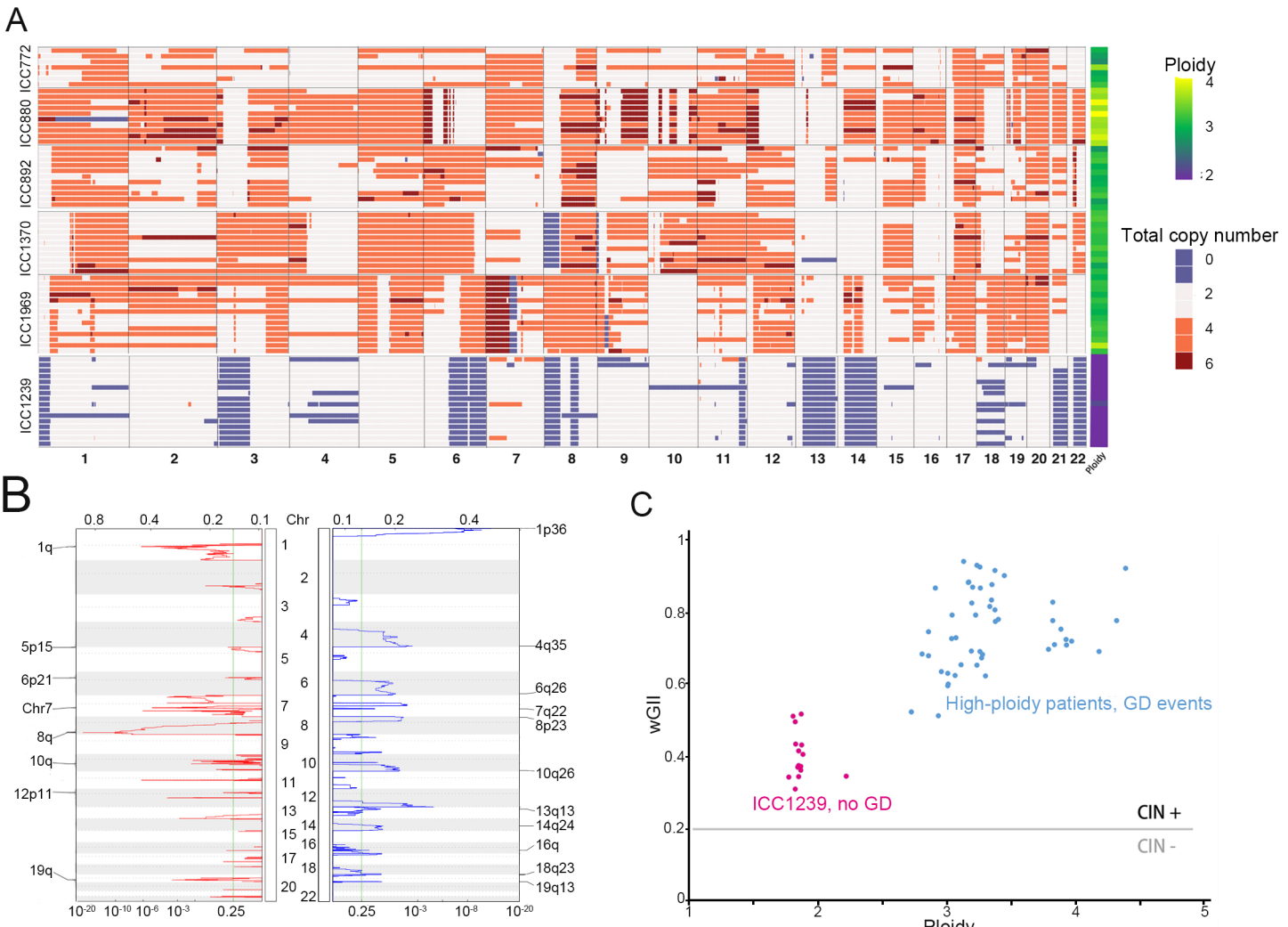
A
ICC772
ICC880
ICC892
ICC1370
ICC1969
ICC1239
1 2 3 4 5 6 7 8 9 10 11 12 13 14 15 16 17 18 19 20 21 22
Ploidy
Ploidy
4
3
2
Total copy number
0
2
4
6
B
0.8 0.4 0.2 0.1
Chr
0.1 0.2 0.4
1q
5p15
6p21
Chr7
8q
10q
12p11
19q
1p36
4q35
6q26
7q22
8p23
10q26
13q13
14q24
16q
18q23
19q13
10-20 10-10 10-6 10-3 0.25
0.25 10-3 10-8 10-20
C
wGII
Ploidy
High-ploidy patients, GD events
ICC1239, no GD
CIN +
CIN -

Figure 5

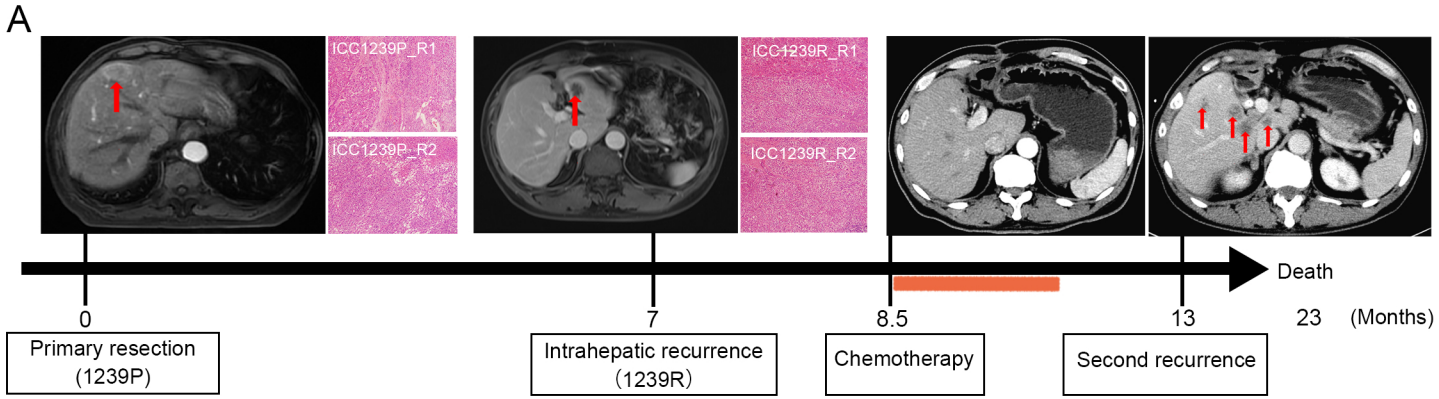
A
ICC1239P_R1
ICC1239P_R2
ICC1239R_R1
ICC1239R_R2
Death
0
7
8.5
13
23
(Months)
Primary resection (1239P)
Intrahepatic recurrence (1239R)
Chemotherapy
Second recurrence

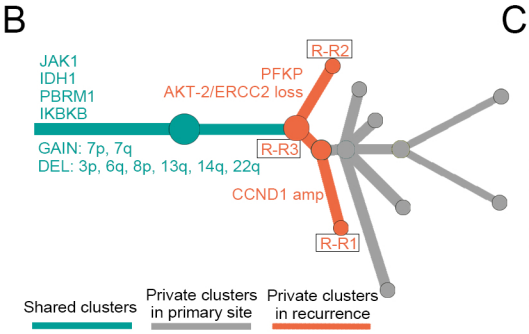
B
JAK1
IDH1
PBRM1
IKBKB
GAIN: 7p, 7q
DEL: 3p, 6q, 8p, 13q, 14q, 22q
PFKP
AKT-2/ERCC2 loss
CCND1 amp
R-R2
R-R3
R-R1
Shared clusters
Private clusters in primary site
Private clusters in recurrence

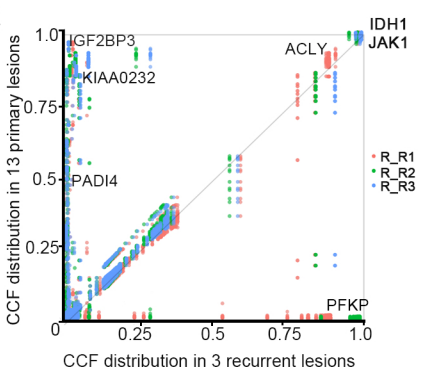
C
IGF2BP3
KIAA0232
PADI4
ACLY
IDH1
JAK1
PFKP
R_R1
R_R2
R_R3
CCF distribution in 13 primary lesions
CCF distribution in 3 recurrent lesions

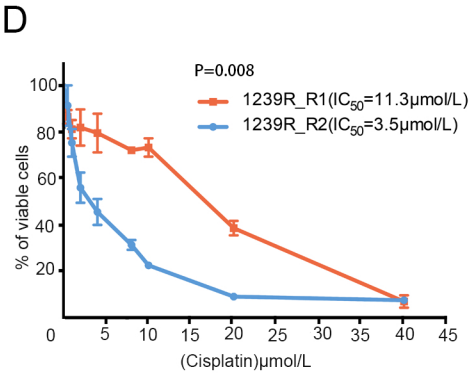
D
P=0.008
1239R_R1(IC50=11.3μmol/L)
1239R_R2(IC50=3.5μmol/L)
% of viable cells
(Cisplatin)μmol/L

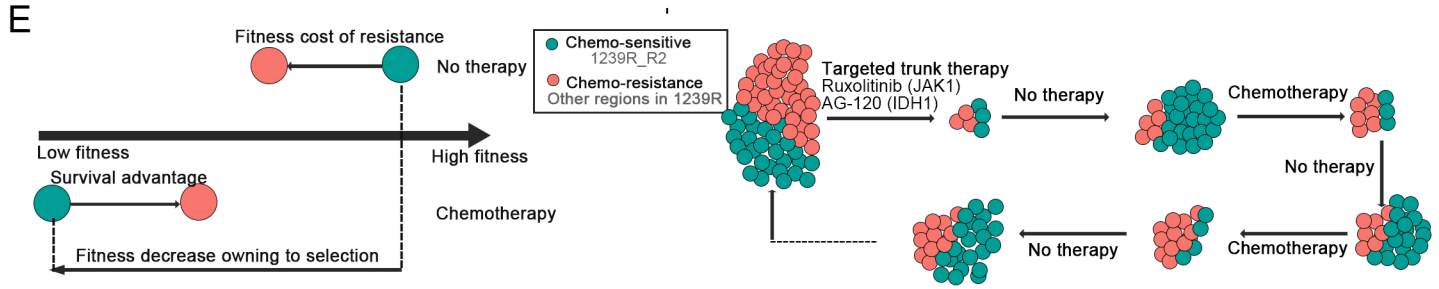
E
Fitness cost of resistance
No therapy
Low fitness
Survival advantage
High fitness
Chemotherapy
Fitness decrease owning to selection
Chemo-sensitive
1239R_R2
Chemo-resistance
Other regions in 1239R
Targeted trunk therapy
Ruxolitinib (JAK1)
AG-120 (IDH1)
No therapy
Chemotherapy
No therapy
Chemotherapy
No therapy
Chemotherapy

Figure 6

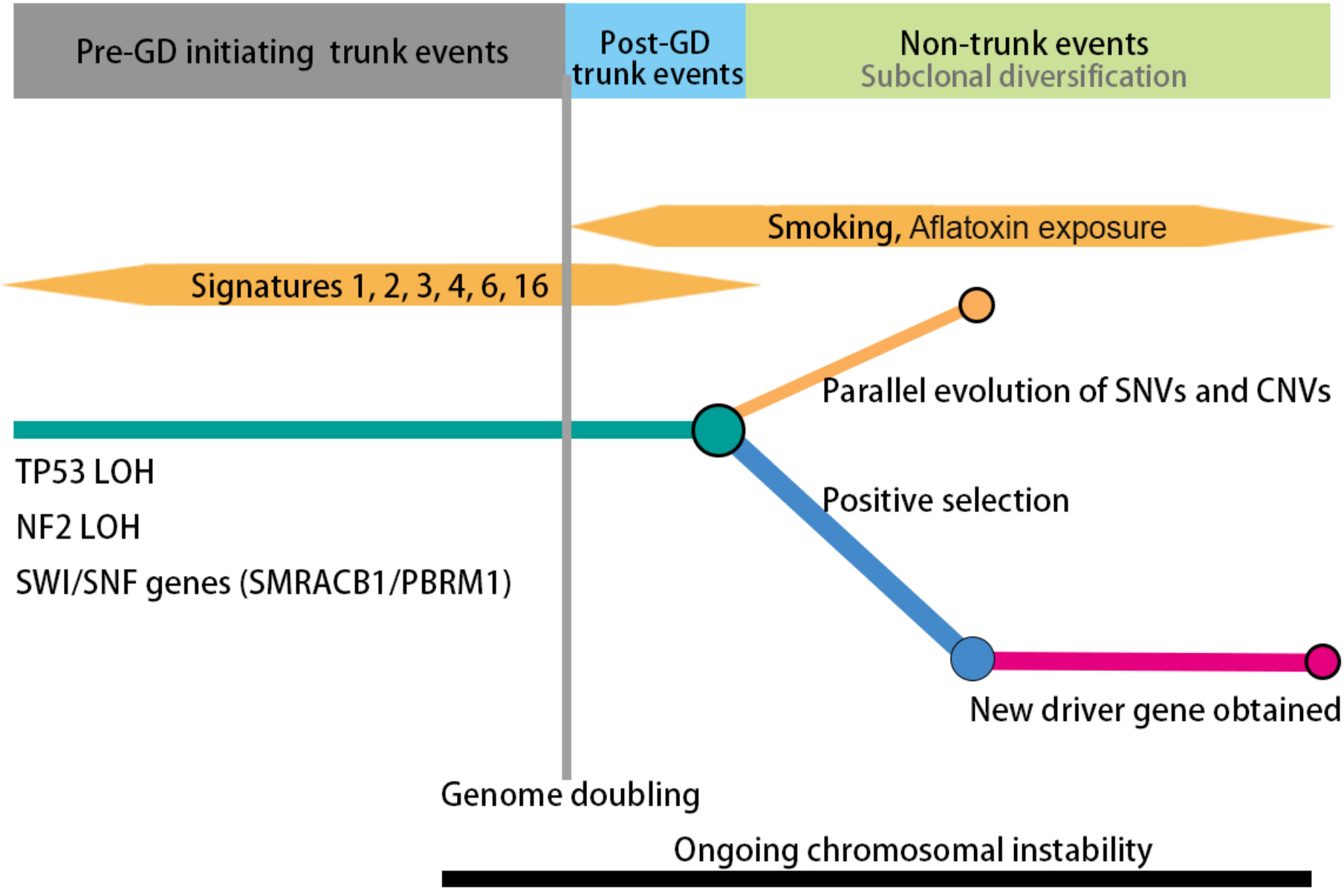
Pre-GD initiating trunk events
Post-GD trunk events
Non-trunk events
Subclonal diversification
Smoking, Aflatoxin exposure
Signatures 1, 2, 3, 4, 6, 16
Parallel evolution of SNVs and CNVs
TP53 LOH
NF2 LOH
SWI/SNF genes (SMRACB1/PBRM1)
Positive selection
New driver gene obtained
Genome doubling
Ongoing chromosomal instability

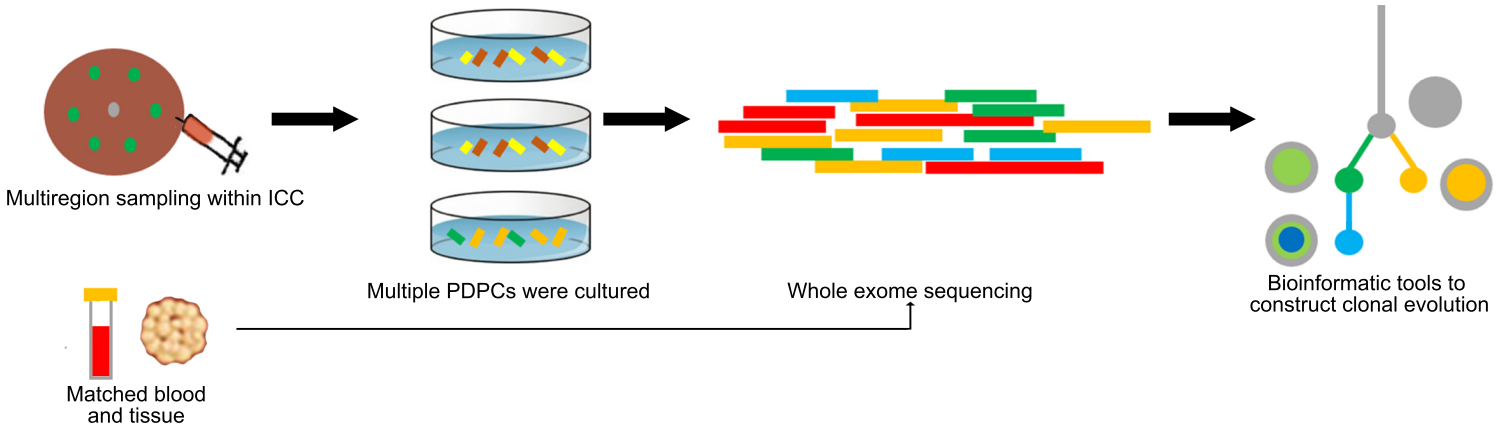
Multiregion sampling within ICC
Multiple PDPCs were cultured
Whole exome sequencing
Bioinformatic tools to construct clonal evolution
Matched blood and tissue